ADVANCED OPTICAL MATERIALS
www.advopticalmat.de

High-Performance Hybrid White OLEDs with Ultra-Stable Emission Color and Small Efficiency Roll-Off Achieved by Incorporating a Deep-Blue Fluorescent Neat Film

Zilong Wu, Xiangyu Zhu, Yinghao Li, Hao Chen, Zeyan Zhuang, Pingchuan Shen, Jiajie Zeng, Jiajin Chi, Dongge Ma, Zujin Zhao, and Ben Zhong Tang*

Organic blue luminescent materials play a vital role in the fabrication of full-color displays and white lighting devices, but high-efficiency blue emitters that meet commercial demands are still quite insufficient. Herein, the authors wish to report the design and synthesis of four bipolar deep-blue luminogens consisting of an anthracene core and various functional groups. Their photophysical properties, electronic structures, electrochemical behavior, thermal stability, carrier transport ability, and electroluminescence performance are systematically studied. The nondoped organic light-emitting diode (OLED) based on DPAC-TAn-BI radiates stable deep-blue light [Commission Internationale de l'Eclairage ($CIE_{x,y}$) = 0.15, 0.15] with a high external quantum efficiency (η_{ext}) of 5.81%. Moreover, efficient two-color hybrid warm white OLEDs are achieved using DPAC-TAn-BI neat film as a blue-emitting layer, providing an excellent η_{ext} of 27.6%, a small efficiency roll-off of 2.9% at 1000 cd m^{-2}, and ultra-stable emission spectra with tiny $CIE_{x,y}$ variation of (0.01, 0.01) from 100 to 10 000 cd m^{-2}. These results demonstrate that the deep-blue luminogens are strong candidates for applications in blue and white OLEDs.

1. Introduction

Organic light-emitting diodes (OLEDs) have attracted intense attention owing to the eminent advantages of high contrast ratio, flexibility, wide viewing angle, low energy consumption, fast response, and so on,[1,2] and have achieved great progress in the applications in solid-state lighting sources and full-color displays. Although certain OLED products have been commercialized in recent years, there are still some bottlenecks frustrating their wide-scale application.[3] One of the key problems is the lack of efficient and robust blue-emitting materials,[4] which play an important role in the RGB (red, green, and blue) display system. Blue luminescent materials with phosphoresce or thermally activated delayed fluorescence are able to realize high electroluminescence (EL) efficiencies but they have to be doped into suitable host materials to alleviate emission quenching and exciton annihilation.[5] These doped devices not only need complicated fabrication process, but also suffer from poor stability and severe efficiency roll-off in most cases. Therefore, it remains a big challenge to develop high-quality blue-emitting materials.[6]

To explore efficient blue-emitting materials, design luminescent molecules with conventional fluorescence may be an effective alternative to obtain high-quality blue emission and improved stability. Due to the suitable wide band gap, anthracene is often used to construct blue-emitting materials with good photoluminescence (PL), based on which highly efficient nondoped deep-blue OLEDs are fabricated.[7] For example, Kim and co-workers reported a novel deep blue emitter based on anthracene and achieved excellent deep blue emissions with a low CIE_y (CIE; Commission Internationale de l'Eclairage) value of 0.06 in nondoped OLED.[6c] Wang and co-workers reported efficient blue emitters consisting of anthracene and functional groups of carbazole and benzonitrile, and realized excellent external quantum efficiency (η_{ext}) values of 10.06% through triplet-triplet annihilation (TTA) process in nondoped OLEDs.[8a] However, in most cases, the rigid and planar structure of anthracene easily leads to strong π–π interaction in the aggregated state, which will result in emission quenching, and thus decreased EL performances.

In this work, we wish to report the design and synthesis of four new deep-blue luminogens based on an anthracene core and various functional groups (**Scheme 1**). The modification

Z. Wu, X. Zhu, Y. Li, H. Chen, Z. Zhuang, P. Shen, J. Zeng, J. Chi, Prof. D. Ma, Prof. Z. Zhao, Prof. B. Z. Tang
State Key Laboratory of Luminescent Materials and Devices
Guangdong Provincial Key Laboratory of Luminescence from Molecular Aggregates
South China University of Technology
Guangzhou 510640, China
E-mail: mszjzhao@scut.edu.cn

Prof. B. Z. Tang
Department of Chemistry
The Hong Kong University of Science & Technology
Clear Water Bay, Kowloon, Hong Kong 999077, China

Prof. B. Z. Tang
AIE Institute
Guangzhou Development District
Huangpu, Guangzhou 510530, China

The ORCID identification number(s) for the author(s) of this article can be found under https://doi.org/10.1002/adom.202100298.

DOI: 10.1002/adom.202100298

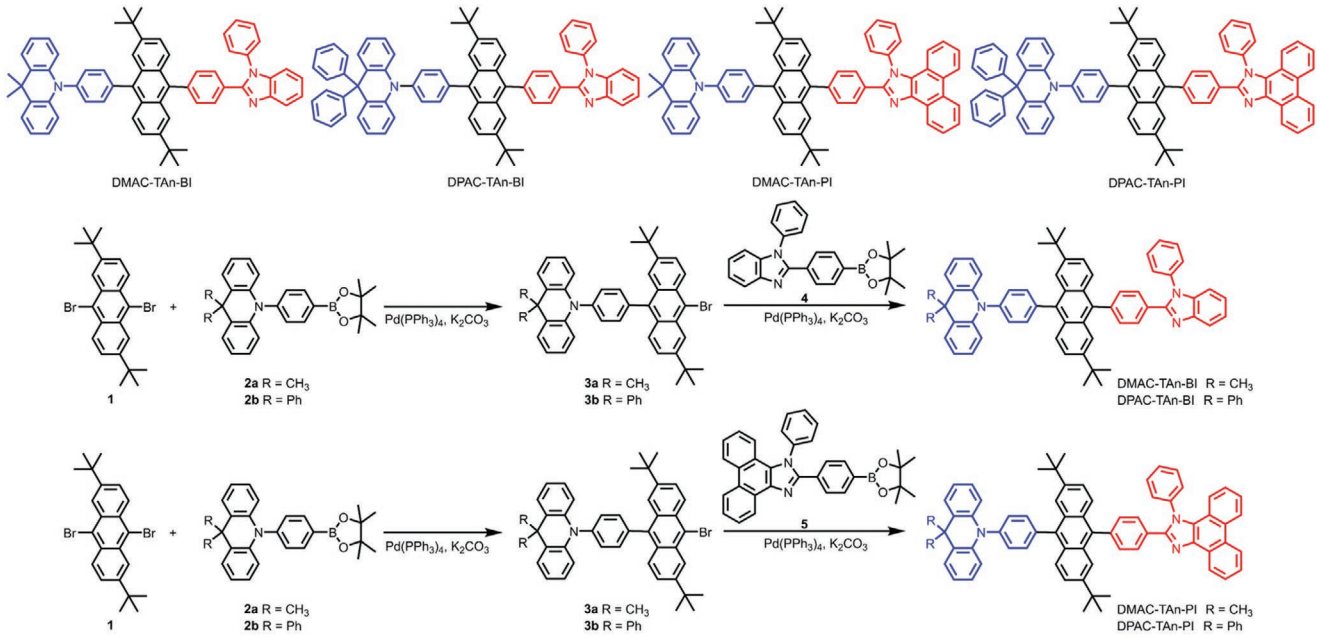

Scheme 1. Molecular structures and synthetic routes toward new deep-blue luminogens.

of branched *tert*-butyl groups on the anthracene core is expected to weaken intermolecular interactions and improve the emission efficiency in the aggregated state.[8b,c] Then, 9,10-dihydro-9,9-dimethylacridine (DMAC) and 9,10-dihydro-9,9-diphenylacridine (DPAC) are introduced to increase hole-transporting ability of the materials.[9] And the methyl and phenyl groups at the 9,9-positions of acridine can be used to modulate molecular packing and intermolecular interactions. In addition, benzoimidazole (BI) and phenanthroimidazole (PI) are further introduced due to their electron-transporting ability, which can balance the injection and transport of carriers in the devices.[10] Although BI and PI are both electron-transporting groups, the different sizes in the molecular planes may induce different optoelectronic properties. These obtained luminogens possess strong deep-blue emissions and bipolar carrier transport ability. Remarkably, they can function efficiently in deep-blue OLEDs and can also be used to create two-color hybrid white OLEDs (WOLEDs)[11] with an excellent η_{ext} of 27.6% and ultra-high spectra stability. These new luminogens are promising deep-blue luminescent materials for OLED application, and the structure-property relationship gained in this work will be useful for further molecular design and functional group selection for blue luminescent materials.

2. Results and Discussion

2.1. Synthesis and Structure

The chemical structures and synthetic routes toward the four new deep-blue luminogens are depicted in Scheme 1. Compounds **1**–**5** were prepared by the reported methods.[9a,10a,12] DMAC-TAn-BI, DPAC-TAn-BI, DMAC-TAn-PI, and DPAC-TAn-PI were synthesized by Suzuki couplings of **3a** and **3b** with **4** and **5** in good yields. All of these new luminogens were purified by column chromatography and then recrystallization. The chemical structures of these luminogens were confirmed by ^{1}H and ^{13}C NMR spectra and high-resolution mass spectrometry. The detailed procedures and characterization data are given in Supporting Information. These luminogens have good solubility in common organic solvents, such as dichloromethane, chloroform, tetrahydrofuran (THF), and toluene.

Single crystals of DPAC-TAn-BI were obtained from the mixture of dichloromethane/ethanol by slow solvent evaporation. As displayed in **Figure 1**A, DPAC-TAn-BI adopts a highly twisted conformation with large dihedral angles of 81.1° and 79.2° between anthracene and the 9,9-positioned phenyl rings. And the phenyl rings at the 9,9-positions of acridine are also twisted out of the plane of acridine. Owing to the twisted

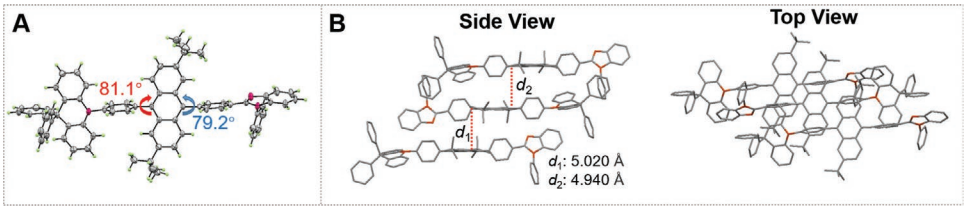

Figure 1. A) The crystal structure and B) packing pattern of DPAC-TAn-BI.

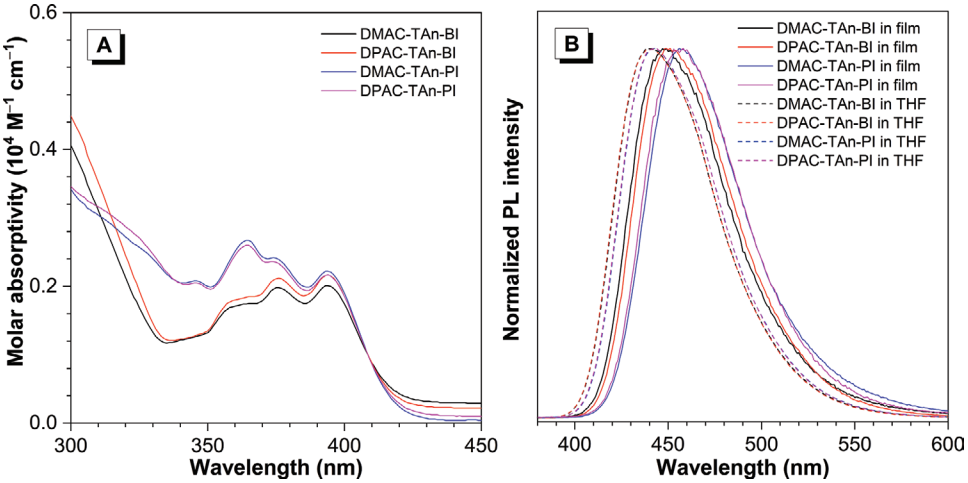

Figure 2. A) Absorption spectra in THF solutions and B) PL spectra in solid neat films and THF solutions of the new deep-blue luminogens.

conformation and branched *tert*-butyl groups, DPAC-TAn-BI molecules are packed loosely in crystals, with long distances of 5.020 Å and 4.940 Å between two adjacent planes of planar anthracene cores, as observed from side view. Moreover, the two adjacent anthracene cores are barely overlapped from top view (Figure 1B). These findings suggest that it is quite difficult for DPAC-TAn-BI to form strong π–π interactions in the aggregated state, which is conducive to achieving high solid-state emission efficiency.

2.2. Photophysical Properties

DMAC-TAn-BI, DPAC-TAn-BI, DMAC-TAn-PI, and DPAC-TAn-PI show identical absorption maxima at 394 nm in dilute THF solutions (10^{-5} M) (**Figure 2**A), which are ascribed to the π–π^* transition of the anthracene core.[7a,b,13] Compared within solutions, these deep-blue luminogens in solid films show almost the same absorption spectra (Figure S1, Supporting Information) except for slight red shifts of ≈5 nm. They can emit intense deep-blue emissions in both dilute solutions and solid films (**Table 1**). The emission peaks in solid films are at 449–458 nm, which are red-shifted ≈10 nm in compared with those in THF solutions as well as those in doped films (441–446 nm) (Figure S2, Supporting Information). They have short fluorescence lifetimes (τ) in solid films (1.22–2.85 ns) and in THF solutions (2.75–3.75 ns). The absolute fluorescence quantum yield (Φ_F) values of DMAC-TAn-BI, DMAC-TAn-PI, and DPAC-TAn-PI are 52.7–71.6% in neat films, and 57.9–65.0% and in doped films with 4,4′-bis(*N*-carbazolyl)-1,1′-biphenyl (CBP) as host, measured by a calibrated integrating sphere (Table 1). Generally, these values are comparable to those in THF solutions, but DPAC-TAn-BI has a higher Φ_F value of 71.6% in neat film, probably due to that the more twisted and branched conformation of DPAC-TAn-BI can better suppress strong intermolecular interactions in neat film, and the intramolecular motion that is vigorous in solution is restricted in neat films, which is also conducive to enhancing emission efficiency.

2.3. Theoretical Calculation

To study the electronic structures, time-dependent density functional theory calculation was carried out with M06-2X/6-31G* and M06-2X/6-311G* basis set.[14] As shown in **Figure 3**, the optimized structures unvain that these luminogens tend to adopt a highly distorted conformation, where the acridine and imidazole are partially distorted out of the anthracene plane. The torsion angles between the anthracene core and the phenyl rings at the 9,10-positions are in the range of 48.57–59.09°, which are smaller than those observed for the crystal structure

Table 1. Photophysical properties, thermal stabilities, and energy levels of the new blue luminogens.

	λ_{abs} [nm]	λ_{em} [nm]	Φ_F[d] [%]	T[e] [ns]	HOMO/LUMO[f] [eV]	T_d [°C]
	Soln[a]/neat film[b]	Soln[a]/neat film[b]/doped film[c]	Soln[a]/neat film[b]/doped film[c]	Soln[a]/neat film[b]		
DMAC-TAn-BI	394/401	439/449/441	64.5/52.7/59.5	3.75/2.85	−5.20/−2.50	446
DPAC-TAn-BI	394/400	439/449/441	66.8/71.6/57.9	3.21/2.56	−5.35/−2.65	494
DMAC-TAn-PI	394/399	443/456/446	68.3/57.3/60.5	2.89/2.26	−5.20/−2.52	460
DPAC-TAn-PI	394/400	442/458/445	70.1/62.3/65.0	2.75/1.22	−5.32/−2.64	501

[a]In THF solution (10^{-5} M); [b]Vacuum-deposited neat film; [c]Vacuum-deposited doped film with CBP host; [d]Absolute fluorescence quantum yield determined by a calibrated integrating sphere; [e]Fluorescence lifetime, measured at room temperature under nitrogen; [f]Determined by CV measurement in solutions.

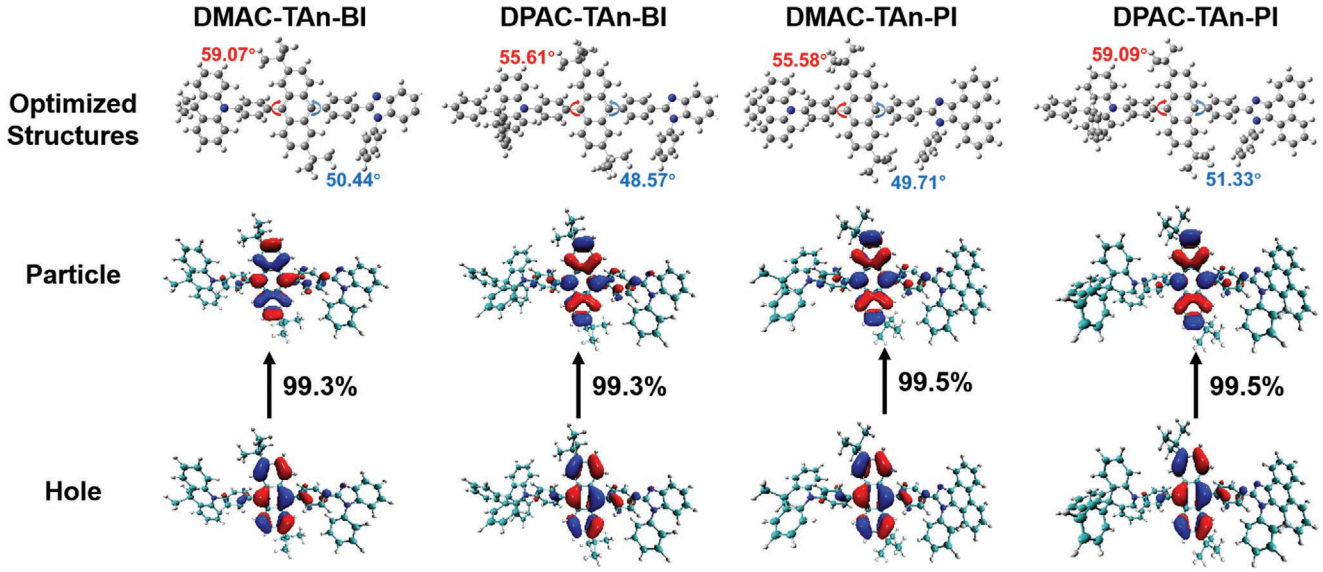

Figure 3. The optimized structures for the S_1 states of the new deep-blue luminogens calculated by M06-2X/6-31G* basis set. Natural transition orbital analysis for the optimized S_1 states calculated by M06-2X/6-311G* basis set.

of DPAC-TAn-BI. These distorted conformations are helpful to prevent the close packing of luminogenic molecules and inhibit the strong intermolecular interaction, which can ensure efficient blue PL emissions in the aggregated state. As shown in Figure 3, the natural transition orbitals of lowest singlet (S_1) states of these luminogens are focused on the anthracene core, and the acridine and imidazole groups show little contributions, indicating the PL emissions are mainly associated with the locally excited state, and the charge transfer excited state can hardly occur in these luminogens.

2.4. Electrochemical Behaviors

In order to evaluate the experimental highest occupied molecular orbital (HOMO) and lowest unoccupied molecular orbital (LUMO) energy levels, the electrochemical behaviors of these deep-blue luminogens were tested by cyclic voltammetry (CV) (**Figure 4**). The results show that these luminogens have partially reversible oxidation and reduction processes. According to the equations of HOMO = $-(E_{ox} + 4.8 - E_{ox,fc})$ eV and LUMO = $-(E_{re} + 4.8 - E_{re,fc})$ eV, where E_{ox} and E_{re} are the onset oxidation and reduction potentials of these blue luminogens, respectively, $E_{ox,fc}$ and $E_{re,fc}$ are the onset oxidation and reduction potentials of Fc/Fc^+, respectively, and 4.8 eV is the hypothetical absolute energy level of Fc/Fc^+ below vacuum,[15] the HOMO energy levels of DMAC-TAn-BI, DPAC-TAn-BI, DMAC-TAn-PI and DPAC-TAn-PI are calculated to be −5.20, −5.35, −5.20 and −5.32 eV, respectively, and the LUMO energy levels are −2.50, −2.65, −2.52 and −2.64 eV, respectively. It can be seen that the LUMO energy levels of these luminogens are higher than that of the electron-transporting material 1,3,5-tri(m-pyrid-3-yl-phenyl)benzene (TmPyPB; −2.7 eV).[16] Therefore, TmPyPB is selected as electron-transporting layer in this work to ensure efficient electron injection.

2.5. Thermal Stability

To fabricate OLEDs by vacuum deposition technology, the thermal stabilities of these blue luminogens are very important, which are examined by the thermogravimetric analysis and differential scanning calorimetry under nitrogen. As shown in Figure S3, Supporting Information, DMAC-TAn-BI, DPAC-TAn-BI, DMAC-TAn-PI and DPAC-TAn-PI have good thermal stabilities with high decomposition temperatures (T_ds) of 446,

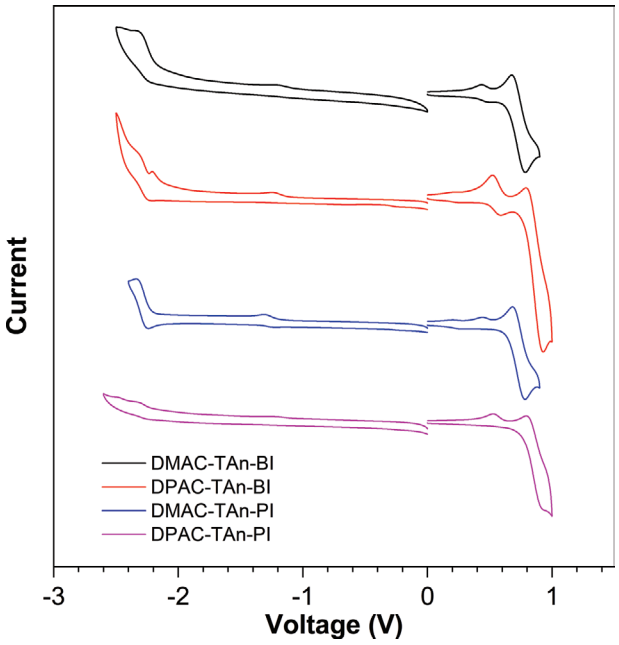

Figure 4. Cyclic voltammograms of the new deep-blue luminogens measured in *N*,*N*-dimethylformamide (negative) and in dichloromethane (positive) containing tetra-*n*-butylammonium hexafluorophosphate (0.1 M).

494, 460, and 501 °C at 5% loss of initial weight, respectively. The obviously higher T_ds of DPAC-TAn-BI and DPAC-TAn-PI than DMAC-TAn-BI and DMAC-TAn-PI indicate DPAC is more favored for improving thermal stability than DMAC. On the other hand, no obvious glass-transition phenomena are observed for these luminogens, demonstrating that they can keep amorphous morphology in a wide range of temperature, which is beneficial to OLEDs application.

2.6. Nondoped and Doped Blue OLEDs

In view of the high thermal stability and good photophysical property of these deep-blue luminogens, they were applied as light-emitting layers for the fabrication of nondoped OLEDs with a configuration of ITO/1,4,5,8,9,11-hexacarbonitrile (HATCN) (5 nm)/di-(4-(*N*,*N*-ditolyl-amino)-phenyl)cyclohexane (TAPC) (50 nm)/tris(4-carbazoyl-9-ylphenyl)amine (TCTA) (5 nm)/emitter (20 nm)/TmPyPB (40 nm)/LiF (1 nm)/Al, in which HTACN, TAPC, TCTA, and TmPyPB functioned as hole injection, hole-transporting, exciton-blocking, and electron-transporting layers, respectively.[16,17] And the selection of these functional layers was mainly based on the consideration of matching energy levels of different layers (**Figure 5**) and improving comprehensive device performance.[7b,17d,18] These devices can be turned on at a low voltage of 3.0 V, and exhibit deep-blue lights with peaks at 448–464 nm (**Table 2**), which are close to the PL peaks in neat films, indicating the exciton recombination mainly occurs within the emissive layers and the EL emissions stem from the decay of singlet excitons. The nondoped device based on DPAC-TAn-BI offers excellent performances, with small $CIE_{x,y}$ values of (0.15, 0.15), and high maximum luminance (L_{max}), current ($\eta_{C,max}$), power ($\eta_{P,max}$), and external quantum efficiencies ($\eta_{ext,max}$) of 2581 cd m^{-2}, 6.48 cd A^{-1}, 6.78 lm W^{-1}, and 5.81%, respectively (**Figure 6** and Table 2). By contrast, the nondoped OLED of DMAC-TAn-BI shows a lower $\eta_{ext,max}$ of 3.17%. Similarly, the device of DPAC-TAn-PI shows a $\eta_{ext,max}$ of 4.45%, while the device of DMAC-TAn-PI gives a lower $\eta_{ext,max}$ of 3.97%. Compared with DMAC, DPAC has a larger space volume, which can better suppress intermolecular π–π interactions, and thus result in larger Φ_F values in neat films of DPAC-TAn-BI and DPAC-TAn-PI than DMAC-TAn-BI and DMAC-TAn-PI. In consequence, the DPAC-TAn-BI and DPAC-TAn-PI exhibit better EL efficiencies. Notably, the outstanding performance of a $\eta_{ext,max}$ as high as 5.81% and deep-blue emission ($CIE_{x,y}$ = 0.15, 0.15) of the device based on DPAC-TAn-BI has surpassed those of many conventional nondoped deep-blue fluorescent OLEDs in the literatures (Table S1, Supporting Information).[8b,c,19–21]

In order to decipher the working mechanism of the excellent EL efficiency of the nondoped OLED based on DPAC-TAn-BI, the magneto- EL (MEL) response in DPAC-TAn-BI-based OLED at different applied voltages and magnetic fields was investigated. As shown in Figure 6D, the MEL curves are increased sharply under low applied magnetic fields (0–50 mT) and decreased slightly under high applied magnetic fields (50–300 mT). What's more, the curves of MEL are enhanced along with the increase of voltages. These results indicate a change in the populations of singlet and triplet excitons, and according to the previous studies,[22] such kind of MEL phenomenon evidences the presence of TTA process, which accounts for the higher $\eta_{ext,max}$ value than the theoretical limit for common fluorescence material.

Moreover, doped OLEDs are also fabricated using the doped films of these luminogens in CBP host as light-emitting layers. The multilayer doped OLEDs have a configuration of ITO/HATCN (5 nm)/TAPC (50 nm)/TCTA (5 nm)/10 wt% emitter: CBP (20 nm)/TmPyPB (40 nm)/LiF (1 nm)/Al. As shown in Table 2 and Figure S4, Supporting Information, the doped devices based on DMAC-TAn-BI, DPAC-TAn-BI, DMAC-TAn-PI, and DPAC-TAn-PI exhibit blue-shifted EL peaks in the range of 436–446 nm with good η_{ext}s of 3.89%, 5.03%, 4.22%, and 4.61%, respectively. The EL performances of DMAC-TAn-BI, DMAC-TAn-PI and DPAC-TAn-PI are improved, partially due to the decreased intermolecular interactions and enhanced Φ_F values in doped films. However, the EL performance of DPAC-TAn-BI is reduced because of the decreased Φ_F value. These doped devices exhibit a low CIE_y coordinate of ≈0.10, which is beneficial for achieving high-quality deep-blue light. The EL spectra of the doped devices are blue-shifted relative to those of nondoped devices because of the bluer PL emissions in doped films than in neat films. These results reveal that, in addition to nondoped OLEDs, these new luminogens can also perform well in doped OLEDs with bluer EL emissions.

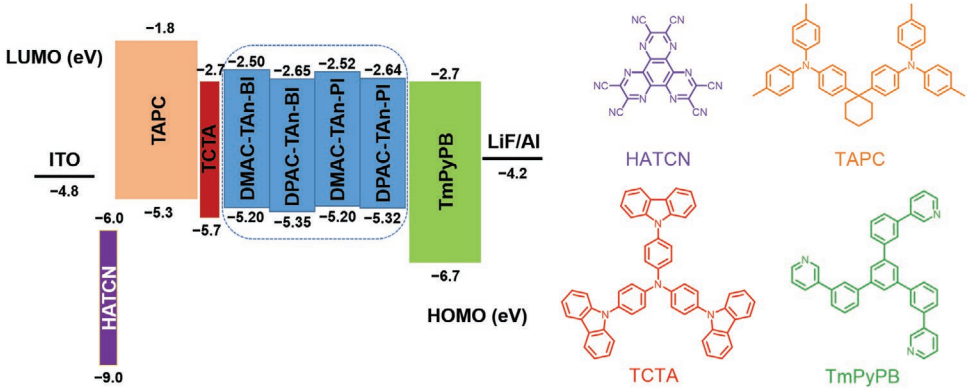

Figure 5. Energy level diagrams of nondoped blue OLEDs based on the new luminogens.

Table 2. The key data of blue OLEDs based on the new luminogens.

Emitter[a)]	V_{on} [V]	L_{max} [cd m^{-2}]	$\eta_{C,max}$ [cd A^{-1}]	$\eta_{P,max}$ [lm W^{-1}]	$\eta_{ext,max}$ [%]	CIE (x,y)	λ_{EL} [nm]
Nondoped OLEDs							
DMAC-TAn-BI	3.0	1628	3.79	3.23	3.17	(0.16, 0.16)	448
DPAC-TAn-BI	3.0	2581	6.48	6.78	5.81	(0.15, 0.15)	450
DMAC-TAn-PI	3.0	5051	5.64	5.91	3.97	(0.16, 0.19)	454
DPAC-TAn-PI	3.0	2784	6.81	6.29	4.45	(0.15, 0.17)	464
Doped OLEDs							
DMAC-TAn-BI	3.0	3624	3.12	2.88	3.89	(0.14, 0.10)	442
DPAC-TAn-BI	3.2	3493	4.53	3.96	5.03	(0.15, 0.10)	446
DMAC-TAn-PI	3.0	6261	3.56	3.29	4.22	(0.15, 0.10)	436
DPAC-TAn-PI	3.0	4552	4.69	3.87	4.61	(0.15, 0.12)	446

[a)]Abbreviation: V_{on} = turn-on voltage at 1 cd m^{-2}; L_{max} = maximum luminance; $\eta_{C,max}$ = maximum current efficiency; $\eta_{P,max}$ = maximum power efficiency; $\eta_{ext,max}$ = maximum external quantum efficiency; CIE = Commission Internationale de l'Eclairage coordinates at 1000 cd m^{-2}; λ_{EL} = electroluminescence peak at 1000 cd m^{-2}.

2.7. Bipolar Carrier Transport

To better understand the excellent EL performance, the space charge limited current (SCLC)[23] method was used to explore the carrier transport capability of these deep-blue luminogens. A series of electron- and hole-only devices were fabricated with configurations of ITO/TmPyPB (10 nm)/emitter (80 nm)/TmPyPB (10 nm)/LiF (1 nm)/Al and ITO/TAPC (10 nm)/emitter (80 nm)/TAPC (10 nm)/Al, respectively. Generally, the characteristics of SCLC can be described by a series of equations as shown in Supporting Information. By fitting the current density–voltage (J–V) curves (**Figure 7**A) in SCLC area, the carrier transport properties of these luminogens are obtained. At an electric field of 5.5×10^5 V cm^{-1}, the electron mobilities of

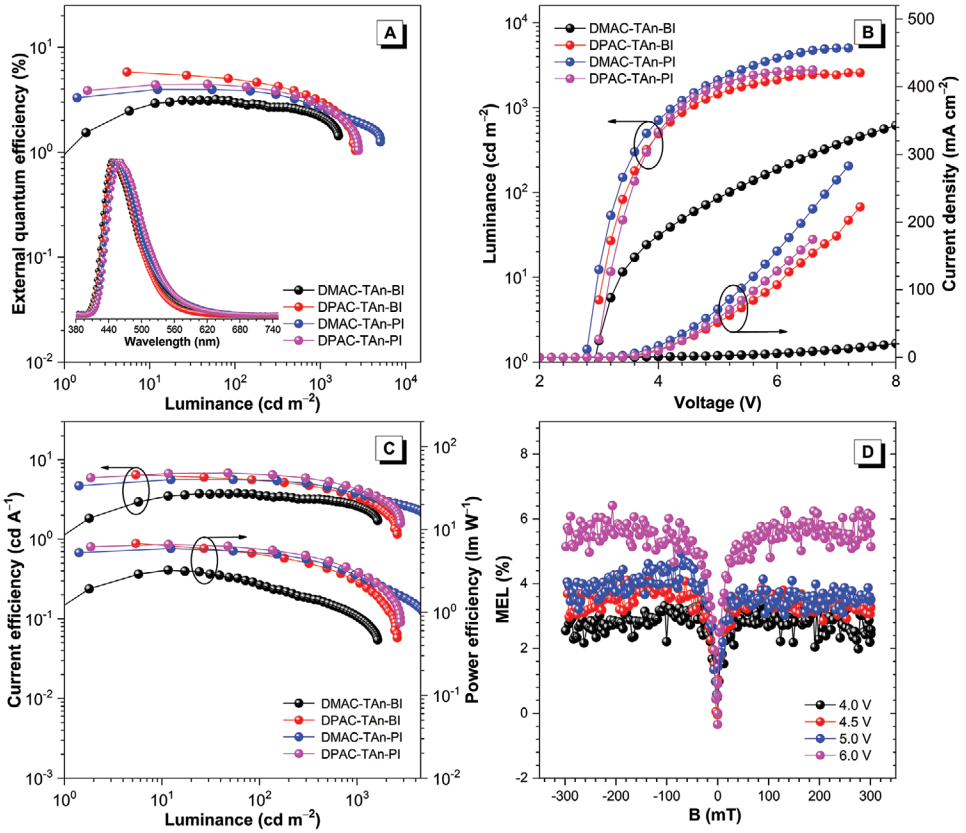

Figure 6. Plots of A) external quantum efficiency–luminance, B) luminance–voltage–current density, and C) current efficiency–luminance–power efficiency of nondoped devices. Inset graph: EL spectra of nondoped devices at 1000 cd m^{-2}. D) MEL responses of the nondoped OLED of DPAC-TAn-BI at different applied voltages.

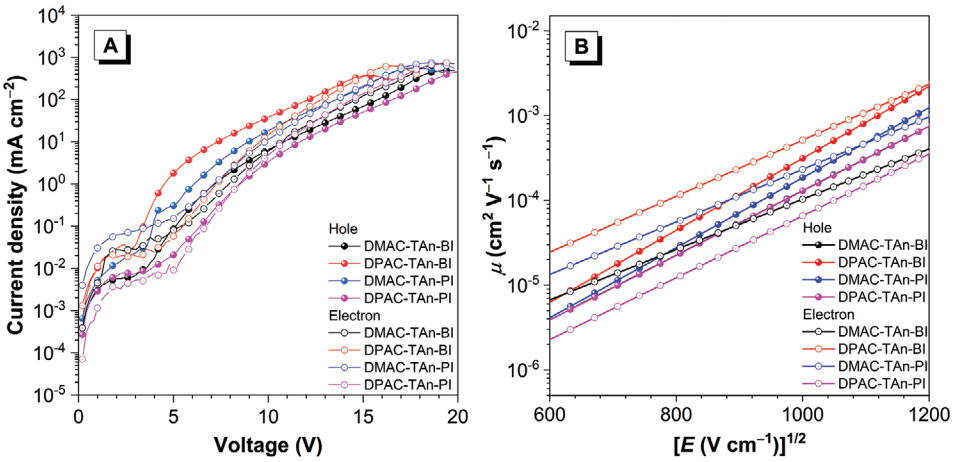

Figure 7. A) Plots of current density–voltage of electron- and hole-only devices based on the new luminogens. B) Electric field-dependent mobilities (μ) of the new luminogens.

DMAC-TAn-BI, DPAC-TAn-BI, DMAC-TAn-PI, and DPAC-TAn-PI are determined to be 1.77×10^{-5}, 7.20×10^{-5}, 3.68×10^{-5}, and 7.50×10^{-6} cm^2 V^{-1} s^{-1}, respectively, while the hole mobilities are 1.35×10^{-5}, 2.51×10^{-5}, 1.59×10^{-5} and 9.53×10^{-6} cm^2 V^{-1} s^{-1} under the same condition, respectively. Obviously, these deep-blue luminogens show comparable hole and electron transport abilities, which is beneficial to the EL performances.

2.8. Two-Color Hybrid WOLEDs

Encouraged by the excellent performance of DPAC-TAn-BI in deep-blue OLEDs, it was used as blue-emitting layer to fabricate two-color hybrid WOLEDs,[24] with the configuration of ITO/HATCN (5 nm)/TAPC (50 nm)/TCTA (5 nm)/50 wt% TCTA: 47 wt% Bepp$_2$: 3 wt% Ir(tptpy)$_2$acac (12 nm)/interlayer (TCTA) (3 nm)/DPAC-TAn-BI (8 nm)/TmPyPB (40 nm)/LiF (1 nm)/Al (device W1) (**Figure 8**E). In the device configuration design, an efficient yellow phosphor, iridium(III) bis(4-(4-*tert*-butylphenyl) thieno[3,2-C]pyridinato-N,C2′) acetylacetonate (Ir(tptpy)$_2$acac) was selected to combine with DPAC-TAn-BI to achieve white light.[8c] Ir(tptpy)$_2$acac was doped into a mixture of TCTA and Bepp2 (bis[2-(2-hydroxyphenyl)-pyridine] beryllium) at a weight ratio of 0.50: 0.47: 0.03 to reduce exciton quenching.[25] TCTA was employed as the interlayer to block energy transfer between DPAC-TAn-BI and Ir(tptpy)$_2$acac, and to regulate the diffusions of carriers and excitons, due to its high triplet energy level (2.76 eV).[24a] The thickness of this interlayer was set to be 3 nm, because this thickness could effectively prevent Dexter energy transfer, which requires a short distance within 1–2 nm, but allow Förster energy transfer, which mainly occurs within ≈3 nm between the fluorophores and phosphors.[18b] Therefore, the triplet excitons could be well confined in the phosphorescent region, resulting in yellow emission. In addition, owing to the high hole mobility (10^{-2} cm^2 V^{-1} s^{-1}) and high LUMO energy level (–1.8 eV), TAPC was adopted as the hole-transporting layer. On the other hand, TmPyPB was chosen as the electron-transporting layer, because of its high electron mobility (10^{-3} cm^2 V^{-1} s^{-1}) and deep HOMO energy level (–6.7 eV).[16,18b]

Since DPAC-TAn-BI has a higher electron mobility (7.20×10^{-5} cm^2 V^{-1} s^{-1}) than hole mobility (2.51×10^{-5} cm^2 V^{-1} s^{-1}), the electron-transporting material is removed in the interlayer, and a WOLED (W1) with an interlayer full of TCTA was fabricated. As shown in **Table 3**, the turn-on voltage of device W1 is as low as 2.8 V, and at a high luminance of 1000 cd m^{-2}, the deriving voltage is only 3.4 V. Device W1 exhibits forward-viewing $\eta_{C,max}$, $\eta_{P,max}$, and $\eta_{ext,max}$ values of 87.5 cd A^{-1}, 87.8 lm W^{-1} and 27.6%, respectively, which are comparable to those of the state-of-the-art hybrid WOLEDs without employing light outcoupling enhancement. At a luminance of 1000 cd m^{-2}, the device still has high EL efficiencies of 84.1 cd A^{-1} and 26.8%, respectively, showing an efficiency roll-off as small as 2.9%. Even under a higher luminance of 5000 cd m^{-2}, the EL efficiencies can still maintain at 66.7 cd A^{-1}, and 21.4%. In addition, similar to other two-color hybrid WOLEDs, device W1 has bright warm white emission (CIE$_{x,y}$ = 0.46, 0.48) with a L_{max} of 46 860 cd m^{-2}, which is the healthy artificial lighting in view of its similar chromaticity as the tungsten incandescent lamps and the low blue intensity. It is worth noting that the variation of CIE$_{x,y}$ coordinates is only (0.01, 0.01) from 100 to 10 000 cd m^{-2}, manifesting that device W1 is of ultra-high color stability. In short, device W1 achieves a high $\eta_{ext,max}$ (27.6%), a low efficiency roll-off (2.9% at 1000 cd m^{-2}), healthy and stable color, high luminance, and low driving voltages, which are outstanding among those of two-color hybrid WOLEDs in the literatures (Table S2, Supporting Information).[8b,c,19d,24c,26–29]

In order to further explore the potential performance, by keeping the interlayer thickness and other functional layers unchanged, the thickness ratio of the yellow emitting layer and the blue emitting layer are adjusted from 12 nm: 8 nm to 10 nm: 10 nm, and 6 nm: 14 nm to obtain additional devices W2 and W3, respectively. As shown in **Figure 9**B,C, the blue emissions in the EL spectra are gradually increased with the increase of blue layers. As shown in Table 3, the devices W2 and W3 exhibit $\eta_{ext,max}$ values of 21.6% and 20.3%, respectively, which are lower than that of device W1, probably due to the non-radiative decay of excessive excitons in DPAC-TAn-BI in view of the decreased yellow phosphorescent layers. Although devices W2 and W3 have declined EL efficiencies, their CIE$_{x,y}$ coordinates

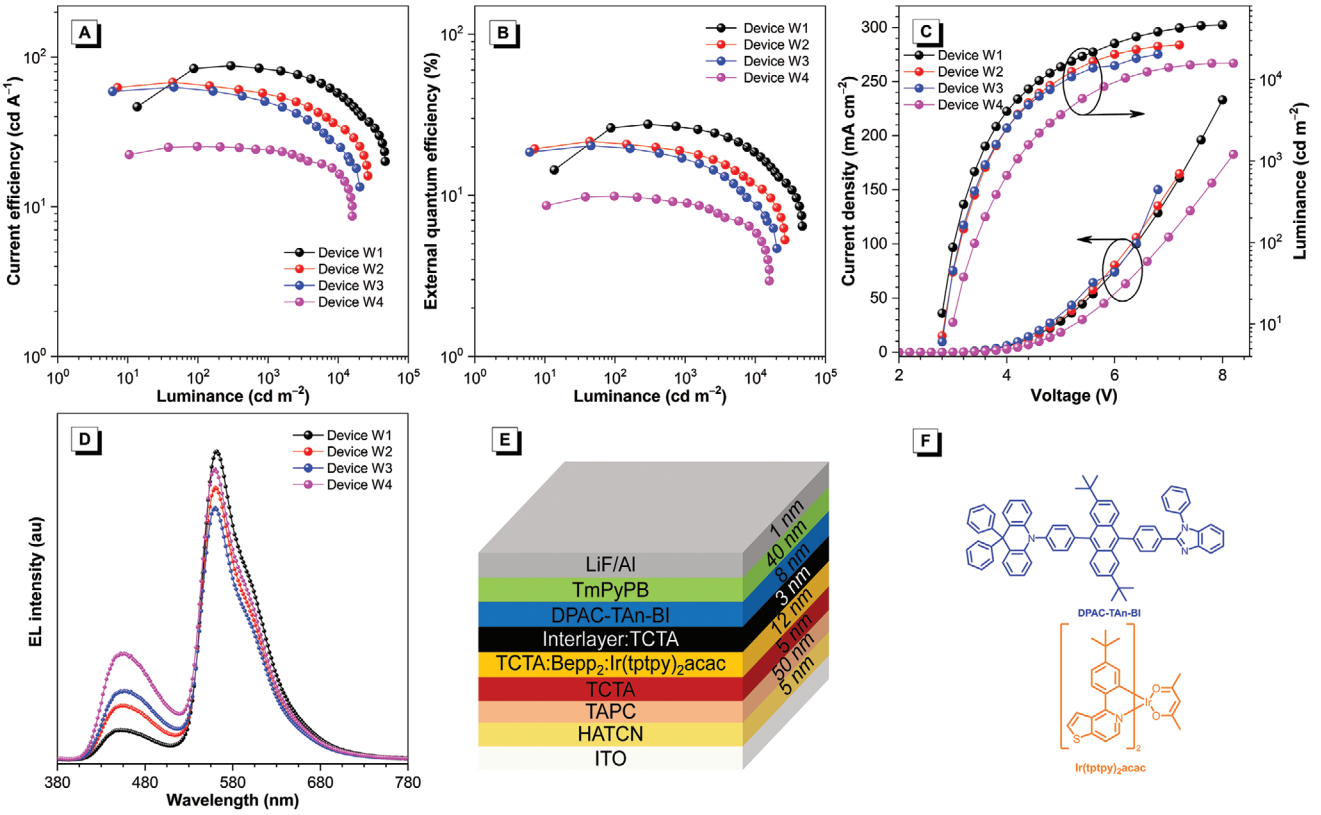

Figure 8. Plots of A) current efficiency–luminance, B) external quantum efficiency–luminance, and C) current density–voltage–luminance of the WOLEDs. D) EL spectra of devices W1–W4 at 5000 cd m^{-2}. E) The schematic configuration of two-color hybrid WOLED (device W1). F) The chemical structures of the blue and yellow emitters.

are improved to (0.42, 0.45) and (0.41, 0.44), respectively, indicating that the emission color can be turned from warm white to pure white by optimizing device structure. Based on the above analyses, to ensure more electrons and holes to recombine within the blue-emitting layer, the TCTA in the interlayer should be increased. Therefore, device W4, whose configuration is the same as that of device W1 but the thickness of the interlayer is increased from 3 to 4 nm, was fabricated. As shown in Figure 9D and Table 3, the CIE$_{x,y}$ coordinates of device W4 are (0.36, 0.38), revealing that pure white light emission is basically achieved, owing to the increased exciton recombination in blue-emitting layer. These results demonstrate that the recombination and distribution of excitons can be effectively modulated by adjusting the components and thickness of the interlayer, which allows the well-tuned color coordinates of white light.

3. Conclusions

In summary, four new deep-blue luminogens (DMAC-TAn-BI, DPAC-TAn-BI, DMAC-TAn-PI, and DPAC-TAn-PI) compromised of a *tert*-butyl modified anthracene core, and acridine and imidazole functional substituents are synthesized and fully characterized. They have high solid-state Φ_F values, good thermal stability, and bipolar carrier transport ability. These new luminogens can be used as light-emitting layers to fabricate deep-blue OLEDs and WOLEDs with excellent performances. The nondoped OLED based on DPAC-TAn-BI radiates stable deep-blue light (CIE$_{x,y}$ = 0.15, 0.15) and excellent EL efficiencies (6.48 cd A^{-1}, 6.78 lm W^{-1}, and 5.81%). Further, high-performance two-color hybrid WOLEDs are fabricated based on DPAC-TAn-BI and Ir(tptpy)$_2$acac. The devices have low turn-on

Table 3. Summary of the performances of two-color hybrid WOLEDs.

Device	V_{on}/V_{1000} [a] [V]	L_{max} [b] [cd m^{-2}]	η_C [c] [cd A^{-1}]	η_P [c] [lm W^{-1}]	η_{ext} [c] [%]	CRI [d]	CIE (x,y) [e]
W1	2.8/3.4	46 860	87.5/84.1/66.7	87.8/78.0/49.9	27.6/26.8/21.4	38	(0.46, 0.48)
W2	2.8/3.6	26 500	67.9/57.6/42.8	71.1/50.1/30.5	21.6/18.9/14.2	43	(0.42, 0.45)
W3	2.8/3.6	20 400	63.0/50.6/34.3	66.1/44.1/24.5	20.3/17.0/11.8	47	(0.41, 0.44)
W4	2.8/4.2	15 840	25.3/24.0/19.3	24.5/17.9/11.2	9.9/9.0/6.9	55	(0.36, 0.38)

[a]The turn-on voltage and the voltage at 1000 cd m^{-2}; [b]Maximum luminance; [c]Order of maximum, then values at 1000 and 5000 cd m^{-2}; [d]Color Rendering Indexes; [e]CIE coordinates at 1000 cd m^{-2}.

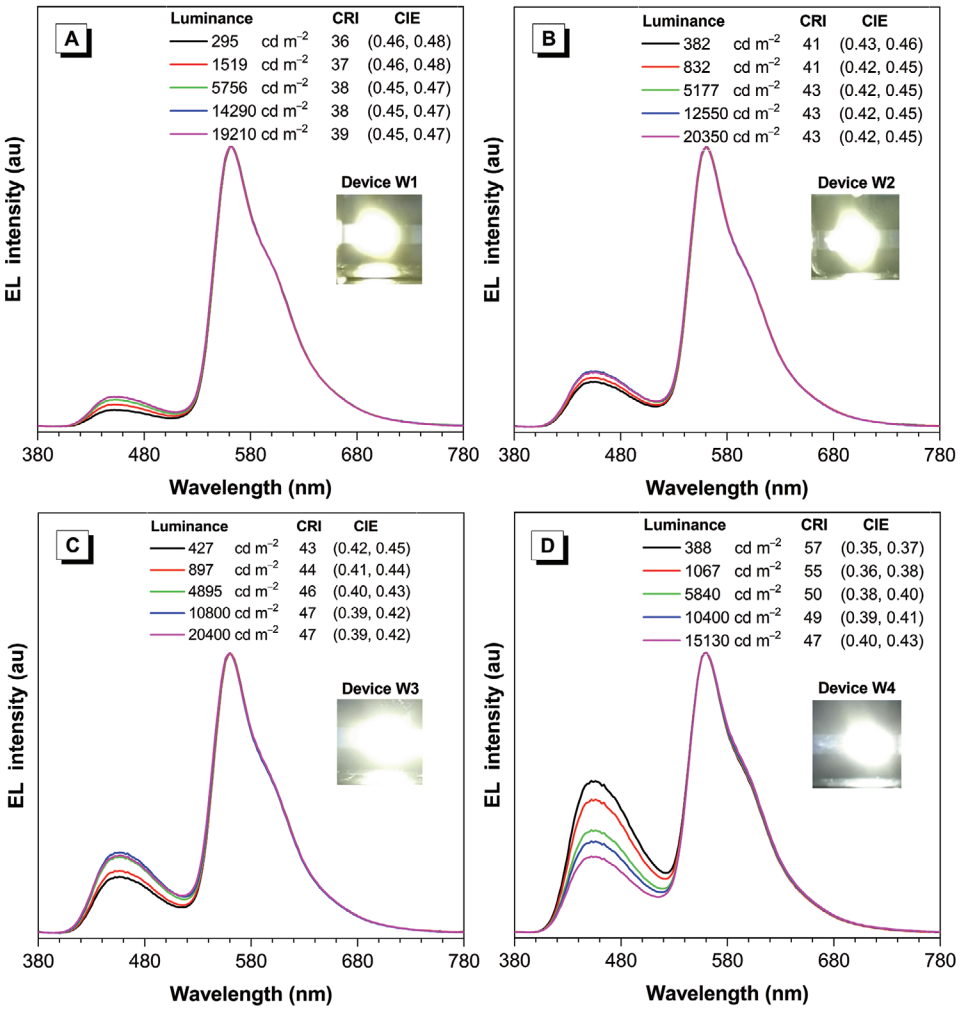

Figure 9. EL spectra of the WOLEDs at varied luminance. Device configuration: ITO/HATCN (5 nm)/TAPC (50 nm)/TCTA (5 nm)/50 wt% TCTA: 47 wt% $Bepp_2$: 3 wt% $Ir(tptpy)_2acac$ (12 nm)/interlayer: TCTA (3 nm)/DPAC-TAn-BI (8 nm)/TmPyPB (40 nm)/LiF (1 nm)/Al (A, device W1); ITO/HATCN (5 nm)/TAPC (50 nm)/TCTA (5 nm)/50 wt% TCTA: 47 wt% $Bepp_2$: 3 wt% $Ir(tptpy)_2acac$ (10 nm)/interlayer: TCTA (3 nm)/DPAC-TAn-BI (10 nm)/TmPyPB (40 nm)/LiF (1 nm)/Al (B, device W2); ITO/HATCN (5 nm)/TAPC (50 nm)/TCTA (5 nm)/50 wt% TCTA: 47 wt% $Bepp_2$: 3 wt% $Ir(tptpy)_2acac$ (6 nm)/interlayer: TCTA (3 nm)/DPAC-TAn-BI (14 nm)/TmPyPB (40 nm)/LiF (1 nm)/Al (C, device W3); ITO/HATCN (5 nm)/TAPC (50 nm)/TCTA (5 nm)/50 wt% TCTA: 47 wt% $Bepp_2$: 3 wt% $Ir(tptpy)_2acac$ (12 nm)/interlayer: TCTA (4 nm)/DPAC-TAn-BI (8 nm)/TmPyPB (40 nm)/LiF (1 nm)/Al (D, device W4).

voltages (2.8 V) and radiate physiologically friendly warm white light ($CIE_{x,y}$ = 0.46, 0.48) with outstanding EL efficiencies (87.8 lm W^{-1} and 27.6%) and a small efficiency roll-off (2.9% at 1000 cd m^{-2}). More importantly, the emission spectra of the WOLEDs are extremely stable, with very small $CIE_{x,y}$ variation of (0.01, 0.01) from 100 to 10 000 cd m^{-2}. To the best of our knowledge, device W1 is among the state-of-the-art two-color hybrid WOLEDs reported so far, demonstrating the broad application prospects in displays and lighting sources of the present deep-blue luminogens.

Supporting Information

Supporting Information is available from the Wiley Online Library or from the author.

Acknowledgements

Z.W. and X.Z. contributed equally to this work. This study was financially supported by the National Natural Science Foundation of China (21788102), the Natural Science Foundation of Guangdong Province (2019B030301003), and the Fundamental Research Funds for the Central Universities.

Conflict of Interest

The authors declare no conflict of interest.

Data Availability Statement

Research data are not shared.

Keywords

anthracene, bipolar carrier transport, blue luminogens, blue organic light-emitting diodes, hybrid white organic light-emitting diodes

Received: February 10, 2021
Revised: April 3, 2021
Published online:

[1] C. W. Tang, S. A. VanSlyke, *Appl. Phys. Lett.* **1987**, *51*, 913.
[2] a) J. Liang, L. Ying, F. Huang, Y. Cao, *J. Mater. Chem. C* **2016**, *4*, 10993; b) Q. Wang, D. Ma, *Chem. Soc. Rev.* **2010**, *39*, 2387; c) G. M. Farinola, R. Ragni, *Chem. Soc. Rev.* **2011**, *40*, 3467.
[3] a) B. Wang, G. Mu, X. Lv, L. Ma, S. Zhuang, L. Wang, *Org. Electron.* **2016**, *34*, 187; b) S. Jhulki, A. K. Mishra, A. Ghosh, T. J. Chow, J. N. Moorthy, *J. Mater. Chem. C* **2016**, *4*, 9310.
[4] S. Reineke, F. Lindner, G. Schwartz, N. Seidler, K. Walzer, B. Lussem, K. Leo, *Nature* **2009**, *459*, 234.
[5] a) Q. Zhang, B. Li, S. Huang, H. Nomura, H. Tanaka, C. Adachi, *Nat. Photonics* **2014**, *8*, 326; b) S. Y. Lee, C. Adachi, T. Yasuda, *Adv. Mater.* **2016**, *28*, 4626.
[6] a) Y. Yuan, J. X. Chen, F. Lu, Q. X. Tong, Q. D. Yang, H. W. Mo, T. W. Ng, F. L. Wong, Z. Q. Guo, J. Ye, Z. Chen, X. H. Zhang, C. S. Lee, *Chem. Mater.* **2013**, *25*, 4957; b) C. Long, G. Lin, H. Peng, S. Ding, W. Luo, R. Hu, S. Chen, H. Fei, A. Qin, Z. Zhao, B. Z. Tang, *Mater. Chem. Front.* **2016**, *1*, 176; c) J. S. Huh, Y. H. Ha, S. K. Kwon, Y. H. Kim, J. J. Kim, *ACS Appl. Mater. Interfaces* **2020**, *12*, 15422; d) J. Zhang, Y. Zhao, H. Xu, D. Zhang, Y. Miao, R. Shinar, J. Shinar, H. Wang, B. Xu, Y. Wu, *J. Mater. Chem. C* **2019**, *7*, 10810.
[7] a) R. Kim, S. Lee, K. H. Kim, Y. J. Lee, S. K. Kwon, J. J. Kim, Y. H. Kim, *Chem. Commun.* **2013**, *49*, 4664; b) B. Liu, H. Nie, X. Zhou, S. Hu, D. Luo, D. Gao, J. Zou, M. Xu, L. Wang, Z. Zhao, A. Qin, J. Peng, H. Ning, Y. Cao, B. Z. Tang, *Adv. Funct. Mater.* **2016**, *26*, 776; c) S. Ye, Y. Wang, R. Guo, Q. Zhang, X. Lv, Y. Duan, P. Leng, S. Sun, L. Wang, *Chem. Eng. J.* **2020**, *393*, 124694; d) Y. Wang, W. Liu, S. Ye, Q. Zhang, Y. Duan, R. Guo, L. Wang, *J. Mater. Chem. C* **2020**, *8*, 9678; e) Y. Xu, X. Liang, Y. Liang, X. Guo, M. Hanif, J. Zhou, X. Zhou, C. Wang, J. Yao, R. Zhao, D. Hu, X. Qiao, D. Ma, Y. Ma, *ACS Appl. Mater. Interfaces* **2019**, *11*, 31139; f) Z. Zhao, S. Chen, C. Y. K. Chan, J. W. Y. Lam, C. K. W. Jim, P. Lu, Z. Chang, H. S. Kwok, H. Qiu, B. Z. Tang, *Chem. - Asian J.* **2012**, *7*, 484.
[8] a) W. Liu, S. Ying, R. Guo, X. Qiao, P. Leng, Q. Zhang, Y. Wang, D. Ma, L. Wang, *J. Mater. Chem. C* **2019**, *7*, 1014; b) B. Chen, B. Liu, J. Zeng, H. Nie, Y. Xiong, J. Zou, H. Ning, Z. Wang, Z. Zhao, B. Z. Tang, *Adv. Funct. Mater.* **2018**, *28*, 1803369; c) Y. Li, Z. Xu, X. Zhu, B. Chen, Z. Wang, B. Xiao, J. W. Y. Lam, Z. Zhao, D. Ma, B. Z. Tang, *ACS Appl. Mater. Interfaces* **2019**, *11*, 17592.
[9] a) X. He, S. Ren, H. Liu, S. Zhao, F. Liu, C. Du, J. Min, H. Zhang, P. Lu, *Chem. - Asian J.* **2020**, *15*, 163; b) X. He, T. Shan, X. Tang, Y. Gao, J. Li, B. Yang, P. Lu, *J. Mater. Chem. C* **2016**, *4*, 10205.
[10] a) X. Tang, Q. Bai, T. Shan, J. Li, Y. Gao, F. Liu, H. Liu, Q. Peng, B. Yang, F. Li, P. Lu, *Adv. Funct. Mater.* **2018**, *28*, 1705813; b) H. Zhang, B. Zhang, Y. Zhang, Z. Xu, H. Wu, P. A. Yin, Z. Wang, Z. Zhao, D. Ma, B. Z. Tang, *Adv. Funct. Mater.* **2020**, *30*, 2002323; c) Z. Wang, P. Lu, S. Chen, Z. Gao, F. Shen, W. Zhang, Y. Xu, H. S. Kwok, Y. Ma, *J. Mater. Chem. C* **2011**, *21*, 5451; d) H. Zhang, J. Zeng, W. Luo, H. Wu, C. Zeng, K. Zhang, W. Feng, Z. Wang, Z. Zhao, B. Z. Tang, *J. Mater. Chem. C* **2019**, *7*, 6359; e) W. Li, D. Liu, F. Shen, D. Ma, Z. Wang, T. Feng, Y. Xu, B. Yang, Y. Ma, *Adv. Funct. Mater.* **2012**, *22*, 2797.
[11] J. Zeng, J. Guo, H. Liu, Z. Zhao, B. Z. Tang, *Adv. Funct. Mater.* **2020**, *30*, 2000019.
[12] a) M. A. Reddy, A. Thomas, K. Srinivas, V. J. Rao, K. Bhanuprakash, B. Sridhar, A. Kumar, M. N. Kamalasanan, R. Srivastava, *J. Mater. Chem. C* **2009**, *19*, 6172; b) S. Hu, J. Zeng, X. Zhu, J. Guo, S. Chen, Z. Zhao, B. Z. Tang, *ACS Appl. Mater. Interfaces* **2019**, *11*, 27134.
[13] a) C. Li, Z. Li, X. Yan, Y. Zhang, Z. Zhang, Y. Wang, *J. Mater. Chem. C* **2017**, *5*, 1973; b) J. Huang, J. H. Su, X. Li, M. K. Lam, K. M. Fung, H. H. Fan, K. W. Cheah, C. H. Chen, H. Tian, *J. Mater. Chem. C* **2011**, *21*, 2957; c) H. Fukagawa, T. Shimizu, N. Ohbe, S. Tokito, K. Tokumaru, H. Fujikake, *Org. Electron.* **2012**, *13*, 1197.
[14] a) J. L. Bredas, *Mater. Horiz.* **2014**, *1*, 17; b) Y. Zhao, D. G. Truhlar, *Theor. Chem. Acc.* **2007**, *120*, 215.
[15] a) S. Tang, W. Li, F. Shen, D. Liu, B. Yang, Y. Ma, *J. Mater. Chem. C* **2012**, *22*, 4401; b) J. W. Jung, J. W. Jo, E. H. Jung, W. H. Jo, *Org. Electron.* **2016**, *31*, 149.
[16] S. J. Su, T. Chiba, T. Takeda, J. Kido, *Adv. Mater.* **2008**, *20*, 2125.
[17] a) X. J. Zhan, N. Sun, Z. B. Wu, J. Tu, L. Yuan, X. Tang, Y. J. Xie, Q. Peng, Y. Q. Dong, Q. Q. Li, D. G. Ma, Z. Li, *Chem. Mater.* **2015**, *27*, 1847; b) L. Ding, Y. Q. Sun, H. Chen, F. S. Zu, Z. K. Wang, L. S. Liao, *J. Mater. Chem. C* **2014**, *2*, 10403; c) J. Chen, F. Zhao, D. Ma, *Mater. Today* **2014**, *17*, 175; d) Y. Tao, C. Yang, J. Qin, *Chem. Soc. Rev.* **2011**, *40*, 2943.
[18] a) B. Liu, H. Nie, G. Lin, S. Hu, D. Gao, J. Zou, M. Xu, L. Wang, Z. Zhao, H. Ning, J. Peng, Y. Cao, B. Z. Tang, *ACS Appl. Mater. Interfaces* **2017**, *9*, 34162; b) B. Liu, X. L. Li, H. Tao, J. Zou, M. Xu, L. Wang, J. Peng, Y. Cao, *J. Mater. Chem. C* **2017**, *5*, 7668.
[19] a) P. I. Shih, C. Y. Chuang, C. H. Chien, E. W. G. Diau, C. F. Shu, *Adv. Funct. Mater.* **2007**, *17*, 3141; b) K. H. Kim, J. Y. Baek, C. W. Cheon, C. K. Moon, B. Sim, M. Y. Choi, J. J. Kim, Y. H. Kim, *Chem. Commun.* **2016**, *52*, 10956; c) F. Liu, H. Liu, X. Tang, S. Ren, X. He, J. Li, C. Du, Z. Feng, P. Lu, *Nano Energy* **2020**, *68*, 104325.
[20] a) J. S. Huh, Y. H. Ha, S. K. Kwon, Y. H. Kim, J. J. Kim, *ACS Appl. Mater. Interfaces* **2020**, *12*, 15422; b) S. O. Kim, K. H. Lee, G. Y. Kim, J. H. Seo, Y. K. Kim, S. S. Yoon, *Synth. Met.* **2010**, *160*, 1259; c) Y. Yu, Z. Wu, Z. Li, B. Jiao, L. Li, L. Ma, D. Wang, G. Zhou, X. Hou, *J. Mater. Chem. C* **2013**, *1*, 8117; d) C. W. Lee, J. G. Jang, M. S. Gong, *Dyes Pigm.* **2013**, *98*, 471.
[21] a) Y. Li, L. Zhou, Y. Jiang, R. Cui, X. Zhao, H. Zhang, *J. Mater. Chem. C* **2017**, *5*, 4219; b) W. C. Chen, Y. Yuan, Y. Xiong, A. L. Rogach, Q. X. Tong, C. S. Lee, *ACS Appl. Mater. Interfaces* **2017**, *9*, 26268; c) Y. Chen, Q. Sun, Y. Dai, D. Yang, X. Qiao, D. Ma, *Adv. Opt. Mater.* **2019**, *7*, 1900703.
[22] a) R. Liu, Y. Zhang, Y. L. Lei, P. Chen, Z. H. Xiong, *J. Appl. Phys.* **2009**, *105*, 093719; b) M. Shao, L. Yan, M. Li, I. Ilia, B. Hu, *J. Mater. Chem. C* **2013**, *1*, 1330; c) Y. Wang, K. Sahin-Tiras, N. J. Harmon, M. Wohlgenannt, M. E. Flatté, *Phys. Rev. X* **2016**, *6*, 011011; d) X. Guo, P. Yuan, X. Qiao, D. Yang, Y. Dai, Q. Sun, A. Qin, B. Z. Tang, D. Ma, *Adv. Funct. Mater.* **2020**, *30*, 1908704.
[23] a) J. Y. Kim, T. Yasuda, Y. S. Yang, C. Adachi, *Adv. Mater.* **2013**, *25*, 2666; b) G. Lin, H. Peng, L. Chen, H. Nie, W. Luo, Y. Li, S. Chen, R. Hu, A. Qin, Z. Zhao, B. Z. Tang, *ACS Appl. Mater. Interfaces* **2016**, *8*, 16799.
[24] a) Y. Sun, N. C. Giebink, H. Kanno, B. Ma, M. E. Thompson, S. R. Forrest, *Nature* **2006**, *440*, 908; b) G. Schwartz, M. Pfeiffer, S. Reineke, K. Walzer, K. Leo, *Adv. Mater.* **2007**, *19*, 3672; c) J. Ye, C. J. Zheng, X. M. Ou, X. H. Zhang, M. K. Fung, C. S. Lee, *Adv. Mater.* **2012**, *24*, 3410; d) N. Sun, Q. Wang, Y. Zhao, Y. Chen, D. Yang, F. Zhao, J. Chen, D. Ma, *Adv. Mater.* **2014**, *26*, 1617.
[25] B. Liu, L. Wang, D. Gao, J. Zou, H. Ning, J. Peng, Y. Cao, *Light: Sci. Appl.* **2016**, *5*, e16137.
[26] a) Z. Chen, X. K. Liu, C. J. Zheng, J. Ye, C. L. Liu, F. Li, X. M. Ou, C. S. Lee, X. H. Zhang, *Chem. Mater.* **2015**, *27*, 5206; b) X. Ouyang, X. L. Li, L. Ai, D. Mi, Z. Ge, S. J. Su, *ACS Appl. Mater. Interfaces* **2015**, *7*, 7869; c) D. Zhang, M. Cai, Y. Zhang, D. Zhang, L. Duan, *ACS Appl. Mater. Interfaces* **2015**, *7*, 28693; d) X. L. Li, X. Ouyang, D. Chen, X. Cai, M. Liu, Z. Ge, Y. Cao, S. J. Su, *Nanotechnology*

2016, *27*, 124001; e) X. Du, G. Li, J. Zhao, S. Tao, C. Zheng, H. Lin, Q. Tong, X. Zhang, *Adv. Opt. Mater.* **2017**, *5*, 1700498.

[27] a) D. Luo, Y. Yang, L. Huang, B. Liu, Y. Zhao, *Dyes Pigm.* **2017**, *147*, 83; b) J. Liang, C. Li, X. Zhuang, K. Ye, Y. Liu, Y. Wang, *Adv. Funct. Mater.* **2018**, *28*, 1707002; c) X. Lv, W. Zhang, D. Ding, C. Han, Z. Huang, S. Xiang, Q. Zhang, H. Xu, L. Wang, *Adv. Opt. Mater.* **2018**, *6*, 1800165; d) S. Ying, J. Yao, Y. Chen, D. Ma, *J. Mater. Chem. C* **2018**, *6*, 7070; e) J. Zhao, Z. Yang, X. Chen, Z. Xie, T. Liu, Z. Chi, Z. Yang, Y. Zhang, M. P. Aldred, Z. Chi, *J. Mater. Chem. C* **2018**, *6*, 4257.

[28] a) C. Cao, W. C. Chen, J. X. Chen, L. Yang, X. Z. Wang, H. Yang, B. Huang, Z. L. Zhu, Q. X. Tong, C. S. Lee, *ACS Appl. Mater. Interfaces* **2019**, *11*, 11691; b) Q. Wang, Y. X. Zhang, Y. Yuan, Y. Hu, Q. S. Tian, Z. Q. Jiang, L. S. Liao, *ACS Appl. Mater. Interfaces* **2019**, *11*, 2197; c) Z. Xu, Y. Gong, Y. Dai, Q. Sun, X. Qiao, D. Yang, X. Zhan, Z. Li, B. Z. Tang, D. Ma, *Adv. Opt. Mater.* **2019**, *7*, 1801539; d) Z. Xu, J. Gu, X. Qiao, A. Qin, B. Z. Tang, D. Ma, *ACS Photonics* **2019**, *6*, 767; e) Y. Chen, D. Yang, X. Qiao, Y. Dai, Q. Sun, D. Ma, *J. Mater. Chem. C* **2020**, *8*, 6577.

[29] a) Y. Chen, J. Zhu, Y. Wu, J. Yao, D. Yang, X. Qiao, Y. Dai, Q. Tong, D. Ma, *J. Mater. Chem. C* **2020**, *8*, 7543; b) P. Han, Z. Xu, C. Lin, D. Ma, A. Qin, B. Z. Tang, *J. Mater. Chem. C* **2020**, *8*, 7012; c) J. Xu, H. Liu, J. Li, Z. Zhao, B. Z. Tang, *Adv. Opt. Mater.* **2021**, *9*, 2001840; d) H. Liu, F. Liu, P. Lu, *J. Mater. Chem. C* **2020**, *8*, 5636.